Efficiency Comparison of Power Converters Based on SiC and GaN Semiconductors at High Switching Frequencies

1st David Lumbreras
Dept. of Electronic Eng. & R&D Power Electronics
Technical University of Catalonia & Circutor, S.A.
Terrassa, Spain
0000-0003-1424-6434

2nd Jordi Zaragoza
Dept. of Electronic Engineering
Technical University of Catalonia
Terrassa, Spain
0000-0002-1463-4560

3rd Néstor Berbel
Dept. of Electronic Engineering
Technical University of Catalonia
Terrassa, Spain
0000-0002-0158-1068

4th Juan Mon
Dept. of Electronic Engineering
Technical University of Catalonia
Terrassa, Spain
0000-0002-2066-4280

5th Eduardo Gálvez
R&D Power Electronics
Circutor, S.A.
Viladecavalls, Spain
0000-0002-0249-2833

6th Alfonso Collado
Technological innovation
Circutor, S.A.
Viladecavalls, Spain
acollado@circutor.com

***Abstract*—Hard-switching voltage source converters (VSC) based on wide-bandgap (WBG) devices surpass their silicon equivalents in every aspect. Nevertheless, at high switching frequencies, the efficiency significantly differs depending on the WBG semiconductor used. This article presents an extensive comparison between gallium nitride (GaN), and silicon carbide (SiC) devices in terms of efficiency. The impact of the switching frequency is evaluated for each semiconductor using two modulation techniques: the classical space vector pulse width modulation (SVPWM) technique, and the innovative hexagonal sigma-delta modulation (H-$\Sigma\Delta$). The performance and losses of both WBG technologies are analysed here using Matlab/Simulink and PLECS. Experimental results performed on two VSC converters, one based on SiC devices and the other made using GaN transistors, show the influence of the semiconductor technology and the modulation strategy on the efficiency at high switching frequencies.**

***Index Terms*—Gallium nitride (GaN), hard-switching, hexagonal quantizer, losses, modulation techniques, PLECS, power electronics, sigma-delta ($\Sigma\Delta$) modulation, silicon carbide (SiC), voltage source converter (VSC), wide-bandgap (WBG) semiconductors.**

I. Introduction

HIGH-FREQUENCY power converters based on wide-bandgap (WBG) semiconductors show superior properties than traditional silicon-based converters. These new power converters exhibit excellent efficiency, may have a high power-density and can operate at extremely high switching frequencies with fewer losses than their silicon counterparts [1], [2]. Silicon carbide (SiC) and gallium nitride (GaN) are the two most mature WBG semiconductors. GaN semiconductors present better features than SiC devices in most parameters, but these devices are currently in its first development stages [3]. Therefore, GaN e-HEMTs are limited to low-voltage applications, while SiC MOSFETs can operate with high voltages [2]. Both technologies have already been successfully used on many power electronics applications, such as: wireless chargers [4], [5], renewable energy [6], [7], onboard EV chargers [8], [9], and ac electric drives [10]. Two-level SiC converters such as voltage source converters (VSC) are becoming the favourite topology in electric vehicles, but GaN converters have also been proposed for this application [11]. Fig. 1 illustrates VSCs based on SiC MOSFETs and GaN e-HEMTs.

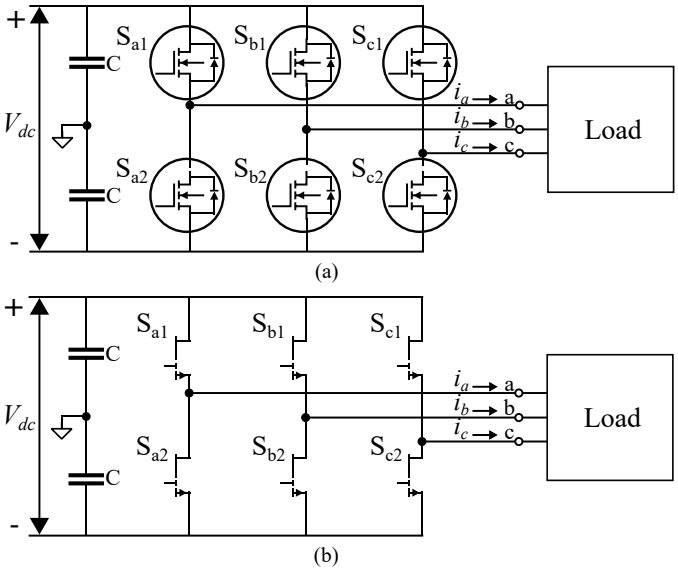

Fig. 1. Voltage source converter based on: (a) SiC MOSFETs; and GaN e-HEMTs.

Although the properties of WBG semiconductors have been

widely analysed, few studies have experimentally compared them. In [12], the authors compare EV battery chargers based on SiC and GaN using a variable switching frequency modulation. In other studies, the efficiency impact of WBG devices is assessed for DC/DC converters [13]. Finally, the losses of six different soft-switched WBG transistors are measured and extensively investigated in [14]. However, all these previous works compare SiC and GaN in DC/DC converters or using soft-switching techniques.

Hard-switched AC/DC converters are common and have many applications. Thus, it is necessary to study the effect of hard-switching modulations in WBG power converters. Usually, VSCs based on WBG devices use the well-known space vector pulse width modulation (SVPWM) or its new variants [10], [15]. These variants may provide significant advantages for WBG converters, such as reducing the common-mode voltage [16] or the deadtime [17]. Nevertheless, PWM techniques have some drawbacks at high switching frequencies: they produce important losses and generate higher low-order harmonics [18]. Recently, new modulation strategies have been proposed to solve these problems, such as the hexagonal sigma-delta modulation (H-ΣΔ) [18], [19]. This technique produces an extreme reduction in switching losses and also mitigates the low-order harmonics in comparison with the classical SVPWM [18].

Relative to our previous work in a conference paper [20], this article is a significant extension of the analysis initially performed. Although our previous article also studies VSC converters, it mainly focuses on three-level power converters and uses different modulation techniques and analysis methods. Furthermore, this previous study only includes simulation results.

This article studies and compares the performance of the most common WBG technologies, i.e. SiC and GaN, in high-frequency VSC converters (see Fig. 1). Moreover, the article analyses the efficiency impact of the switching frequency on the former semiconductors. Since the modulation technique may have a great impact on converter efficiency, the study is performed using two modulation techniques: the classic SVPWM, and the innovative H-ΣΔ. The impact of both semiconductors is evaluated on the basis of simulation studies using the software MATLAB/Simulink and PLECS. Finally, the results are experimentally validated by implementing the proposed techniques on two VSC converters: one made using SiC MOSFETs, and the other based on GaN e-HEMTs.

The rest of this article is organized as follows. Section II introduces the applied modulation strategies. Section III compares the behaviour of the studied WBG power converters. Section IV experimentally validates the previous results using two prototypes. Finally, Section V summarizes the conclusions of this article.

II. Modulation Strategies

The scheme of the applied modulation strategies is depicted in Fig. 2. Fig. 2(a) illustrates the SVPWM scheme. This modulation injects a zero-sequence (V_0) to the original reference

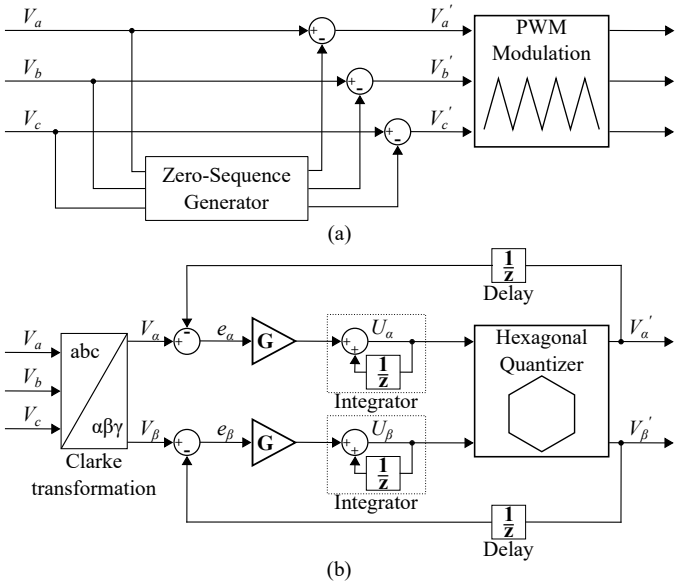

Fig. 2. Modulator loops of: (a) SVPWM; and (b) H-ΣΔ. The nominal value of all gains is unity.

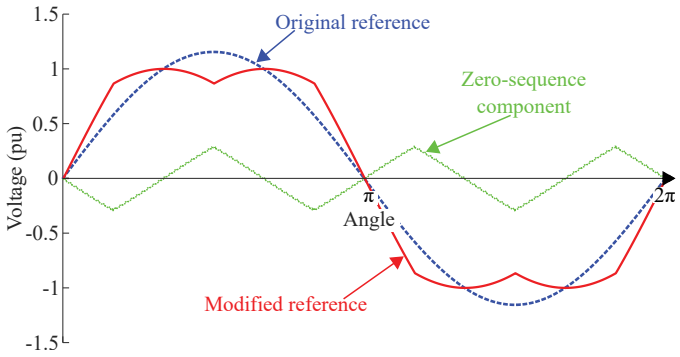

Fig. 3. Space vector pulse width modulation.

signals. The zero-sequence extends by 15% the maximum modulation index [21]. The new modulators are defined using

$$\begin{cases} V_a' = V_a - V_0 \\ V_b' = V_b - V_0, \\ V_c' = V_c - V_0 \end{cases} \tag{1}$$

where

$$V_0 = \frac{\max(V_a, V_b, V_c) + \min(V_a, V_b, V_c)}{2}. \tag{2}$$

Fig. 3 plots the original reference waveform, the zero-sequence component and the modified reference.

Fig. 2(b) shows the H-ΣΔ scheme. The basis of H-ΣΔ is the following [22]: the reference signals (V_α, V_β), expressed in the $\alpha\beta$ frame, are sampled and compared with the current converter output (V_α', V_β'). The error (e_α, e_β) is integrated and then quantized into a digital signal. There are gains before each integration, whose value may be adjusted for guaranteeing low output noise and system stability [18], [23]. The digital signal is the next output of the modulator. Usually,

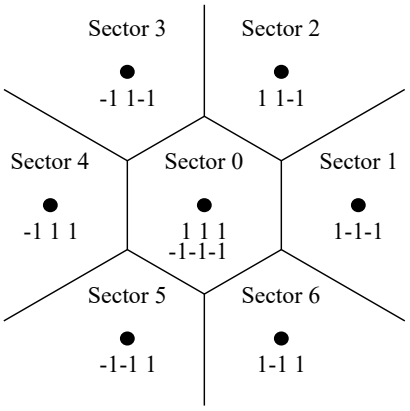

Fig. 4. Voltage space vectors and sector definitions according to a hexagonal quantizer.

there is a quantization error, i.e. the difference between the input and output of the quantizer, but is decreased by oversampling the reference signals [22], [24]. The equation that describes the H-ΣΔ is

$$V_j'(z) = V_j(z)z^{-1} + e_j(z)(1 - z^{-1}) \tag{3}$$

where $j = \{\alpha, \beta\}$.

The core of the H-ΣΔ technique is its hexagonal quantizer. The quantizer divides the $\alpha\beta$ plane into seven sectors (see Fig. 4): one for each active vector and another for the two zero vectors. These vectors are represented by -1 and 1, which indicate, respectively, the output voltage levels of $-V_{dc}/2$ and $V_{dc}/2$ that correspond to the midpoint of the dc bus. At every sampling instant, the hexagonal quantizer determines the position of the input and synthesises it by applying the closest switching vector. The nearest switching vector is found using

$$D_j^2 = (V_{\alpha j}' - U_\alpha)^2 + (V_{\beta j}' - U_\beta)^2 \tag{4}$$

where D_j^2 is the Euclidean distance squared from the integrated error (U_α,U_β) to the switching state ($V_\alpha^{'}$, $V_\beta^{'}$).

The point that is closest to the reference is the switching vector with the minimum value of D_i^2. Branch and bound algorithms can be used to optimize the calculation of the nearest vector [18]. The switching state of the inverter is determined from the output of the quantizer. This procedure is direct, except when the quantizer input is within Sector 0. In this case, the converter can apply either of the two zero vectors. The implemented H-ΣΔ always select the zero vector that minimizes the switchings. Fig. 5 depicts the hexagonal regions, the trajectory of the integrated error and the reference voltage during a period.

An important difference between SVPWM and H-ΣΔ is the switching frequency. This parameter is variable in H-ΣΔ, so this article uses the maximum switching frequency as a comparison parameter. The maximum switching frequency (f_{max}) is defined as follows:

$$f_{max} = \begin{cases} f_{sw} & \text{for SVPWM} \\ f_s/2 & \text{for H-}\Sigma\Delta \end{cases}, \tag{5}$$

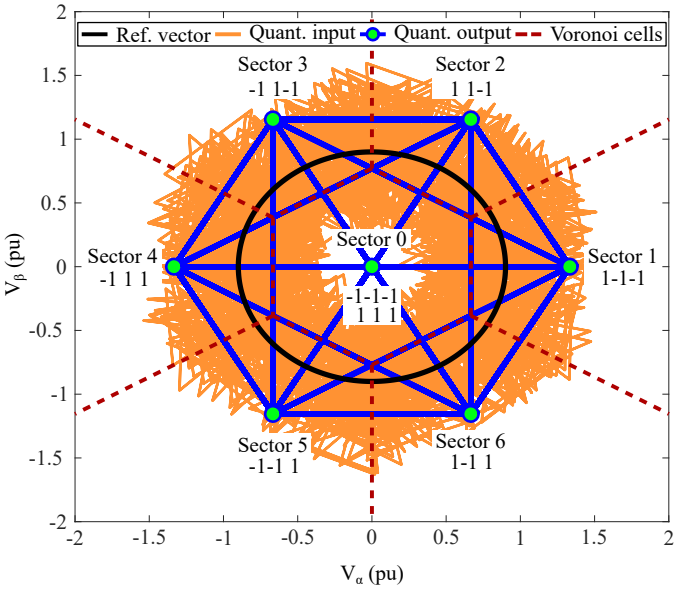

Fig. 5. Trajectory of the reference voltage, the integrated error, and the quantizer output within $\alpha\beta$ plane. The dashed red lines mark the boundaries of the Voronoi's regions. Modulation index: m = 0.9. Maximum frequency: f_{max} = 100 kHz.

where f_{sw} is the switching frequency and f_s is the sampling frequency.

III. Simulation Results

This section evaluates the losses of the studied WBG power converters (see Fig. 1) under various operating conditions. The studied VSCs are modelled using MATLAB/Simulink and PLECS Blockset. The rated power of the converter is 8.81 kVA, the dc bus voltage is 600 V, and the ac-side currents are constant at their rated values (15 A). The SiC converter uses the MOSFET module FS45MR12W1M1_B11. This module features a maximum drain-source voltage (V_{ds}) of 1.2 kV and a continuous drain current (I_d) of 25 A. The GaN VSC employs six GS66508T e-HEMTs. These transistors allow a maximum V_{ds} of 650 V and an I_d of 30 A. The deadtime used in the SiC converter is 200 ns, while the one used in the GaN converter is 40 ns. All the junction temperatures are 125 ºC. The PLECS software calculates the losses according to the thermal datasheet and the equations provided by the manufacturers. The manufacturer of the SiC module does not provide an equation. Hence, this study uses a polynomial approximation to obtain this loss equation, as is detailed in [25].

The total losses are estimated with the converters working at two maximum switching frequencies (f_{max}): 100 and 200 kHz. To compare the total losses at these different frequencies, total loss increase (TLI) is defined as

$$TLI(\%) = 100 \cdot \frac{P_{tl}(200\text{ kHz}) - P_{tl}(100\text{ kHz})}{P_{tl}(100\text{ kHz})} \tag{6}$$

where $P_{tl}(f_{max})$ are the total losses of the converter at f_{max}.

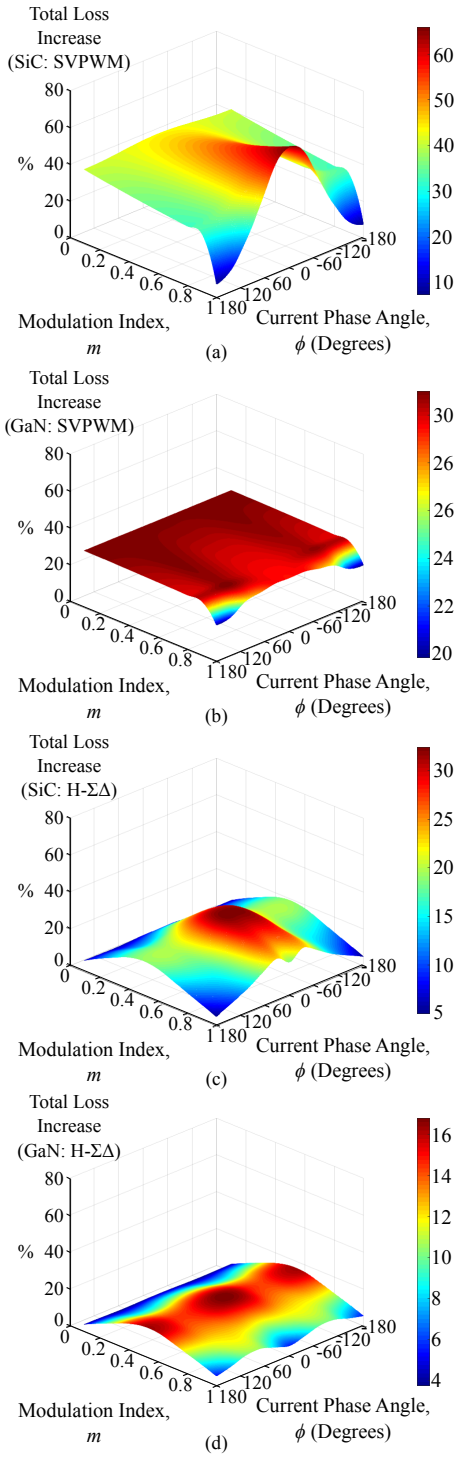

Fig. 6. Total loss increase using: (a) and (b) SVPWM; (c) and (d) H-ΣΔ.

Fig. 6 depicts the total loss increase of the studied WBG power converters. Fig. 6(a) and (b) illustrates the TLI using the SVPWM technique. Fig. 6(a) shows the SiC converter results, while Fig. 6(b) displays the TLI of the GaN converter. At most operating points, SiC produces a TLI between 30 and 40%. However, the loss increase is significantly higher when the current phase angle is 0º. GaN produces less TLI than SiC for most operating points. Moreover, the operating point barely affects the GaN loss increase. The TLI remains around 30% at most operating points. Fig. 6(c) and (d) depicts the results applying the H-ΣΔ strategy using SiC and GaN, respectively. This modulation produces fewer losses than the SVPWM, especially at high switching frequencies. Hence, the produced TLI is lower. Fig. 6(c) illustrates the SiC total loss increase. In general, the TLI is about half of that produced using the SVPWM. However, at low modulation indexes, the H-ΣΔ strategy reduces more the total loss increase. Fig. 6(d) displays the TLI of the GaN converter. The effect of H-ΣΔ on GaN is less noticeable than on SiC since the first produce fewer switching losses. Around $m = 0.7$, the TLI is reduced from 30 to 16%. At all other operating points, the reduction is even higher. Hence, using the H-ΣΔ technique allows doubling the maximum switching frequency without significantly increasing the losses.

IV. Experimental Results

To experimentally evaluate the performance of wide-bandgap power converters (see Fig. 1), we used two scaled-down prototypes. The first prototype incorporates the previously simulated SiC MOSFETs (FS45MR12W1M1_B11). The other one uses the formerly studied GaN e-HEMTs (GS66508T). The deadtimes are 200 and 40 ns for the SiC and the GaN converter, respectively. The SiC converter uses the device ADUM4135BRWZ as driver, while the GaN converter uses the model ADUM4121ARIZ. The two drivers have two drive inputs to control the gate drive signals. Both inputs are used together to protect the transistors in case of noise in the control signals. On the ac side, there was a three-phase series-connected RL load with $R = 68\ \Omega$ and $L = 460\ \mu$H. The dc side of the converter was supplied by a constant 300-Vdc source. The modulation techniques were implemented on a dSPACE DS1006 platform and a DS5203 FPGA board. Voltages, currents and efficiencies were measured with a digital power meter (Yokogawa WT1600: 1 MHz bandwidth). Fig. 7 shows the experimental setup.

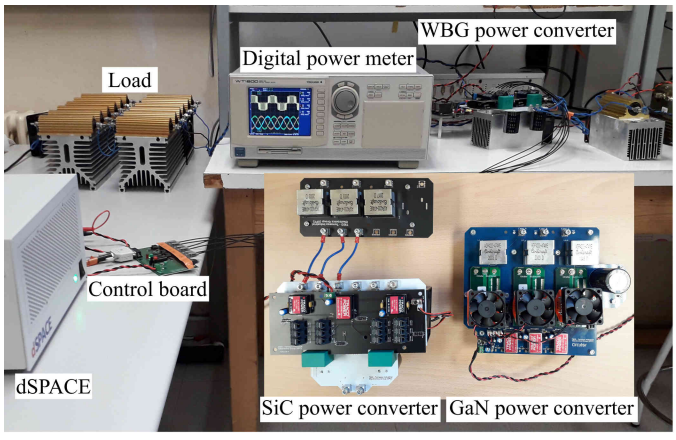

Fig. 7. View of the WBG power converters and the experimental setup.

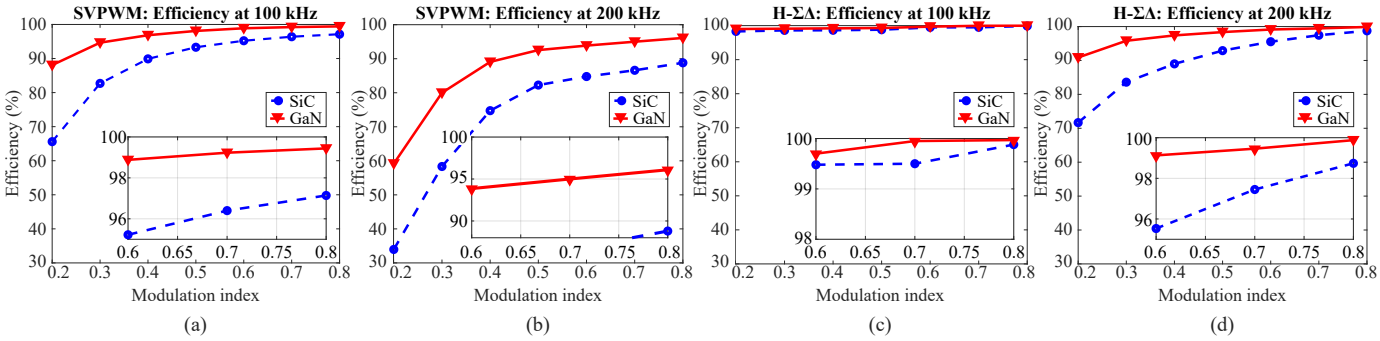

Fig. 8. Experimental converter efficiency curves using: (a) and (b) SVPWM; (c) and (d) H-ΣΔ.

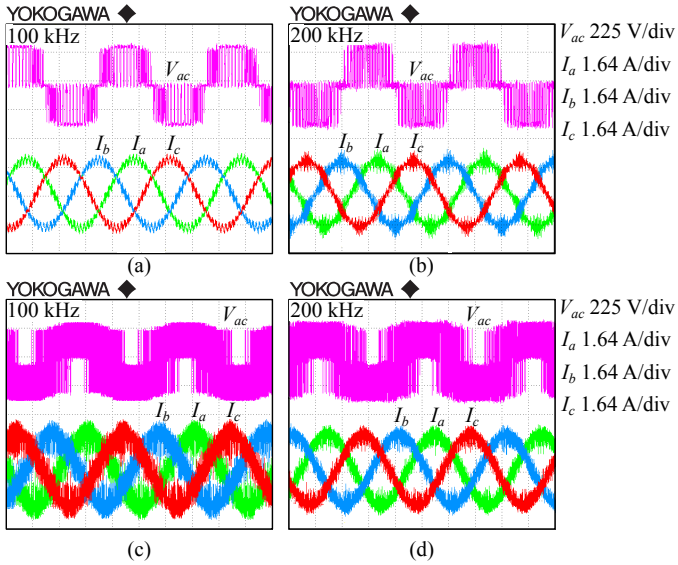

Fig. 9. Experimental waveforms obtained at high frequency and m = 0.8 using: (a) and (b) SVPWM; (c) and (d) H-ΣΔ.

Fig. 8 depicts the efficiencies of both converters when using the two modulations at 100 and 200 kHz. Fig. 8(a) illustrates the performance at 100 kHz applying the SVPWM strategy. The performance of both converters increases along with the modulation index. Although GaN always shows higher efficiencies than SiC, the difference between efficiencies reaches a minimum for high modulation indexes. At these indexes, SiC shows a performance of around 97% and GaN exhibits an efficiency of 99.4%. Fig. 8(b) plots the results at 200 kHz using SVPWM. At this frequency, both converters have the same behaviour as at 100 kHz. The two converters are less efficient at 200 kHz because of their higher number of switchings. However, the difference between the efficiency of SiC and GaN is more significant, since the first produces more switching losses. In this scenario, the maximum efficiency of SiC is 88.8%, whereas GaN has a maximum performance of 96.1%. Fig. 8(c) shows the efficiency at 100 kHz using the H-ΣΔ technique. Under these conditions, the operating point barely affects performance. The efficiency of both converters is similar and always greater than 99%, but GaN shows slightly higher performance than SiC. Fig. 8(d) depicts the results at 200 kHz using H-ΣΔ. In this scenario, both converters exhibit superior efficiencies than those of SVPWM at 100 kHz. The maximum performance is produced at high modulation indexes. The highest efficiency of SiC is 98.74%, while the GaN maximum performance is higher than 99%.

Fig. 9 plots the line voltages (V_{ac}) and the output currents (I_a, I_b, I_c) produced by the SiC converter. Since the GaN VSC produces the same waveforms, these results are not included. Fig. 9(a) and (b) illustrates the waveforms obtained using the SVPWM strategy at 100 and 200 kHz, respectively. The converter produces three balanced sinusoidal output currents. At 200 kHz, the output currents have slightly more ripple than at 100 kHz since there are higher low-order harmonics [21]. There are no significant differences between the line voltage at 100 and 200 kHz. Fig. 9(c) and (d) shows the results applying the H-ΣΔ technique at 100 and 200 kHz. The output currents are balanced and sinusoidal but have more ripple than those of the SVPWM. Nevertheless, increasing the maximum switching frequency produces a significant reduction on the output current ripple. Including a second integrator loop in the ΣΔ also decreases the current ripple and the low-order harmonics [18]. The line voltage is similar at the two studied frequencies, but the SVPWM technique produces cleaner voltages than H-ΣΔ since the later may switch two phases at once.

V. Conclusion

This article compares the efficiency of SiC and GaN semiconductors in high-frequency power converters. The benefits of both technologies are demonstrated by simulation and experimental results. The results show that GaN converters always exhibit better performance than SiC VSCs. Applying the SVPWM technique, the efficiency of SiC converters considerably decreases as the switching frequency increases. Since GaN produces fewer switching losses, the switching frequency has less impact on GaN converters. The efficiency of both converters is greatly improved when they use the H-ΣΔ strategy. The experiments demonstrate that H-ΣΔ modulation allows high-frequency operation with few power losses. GaN has the best performance despite the modulation. Finally, this article concludes that high-frequency modulation techniques are needed for taking advantage of WBG power converters.

ACKNOWLEDGMENT

This work was supported by the Industrial Doctorates Plan of the Secretaria d'Universitats i Recerca del Departament d'Empresa i Coneixement de la Generalitat de Catalunya, and the Ministerio de Ciencia, Innovación y Universidades of Spain within the project PID2019-111420RB-I00.

REFERENCES

[1] J. Millan, P. Godignon, X. Perpina, A. Perez-Tomas, and J. Rebollo, "A survey of wide bandgap power semiconductor devices," *IEEE Transactions on Power Electronics*, vol. 29, no. 5, pp. 2155–2163, May 2014.

[2] K. Shenai, "High-Density Power Conversion and Wide- Bandgap Semiconductor Power Electronics Switching Devices," *Proceedings of the IEEE*, vol. 107, no. 12, pp. 1–19, Nov. 2019.

[3] I. López, E. Ibarra, A. Matallana, J. Andreu, and I. Kortabarria, "Next generation electric drives for HEV/EV propulsion systems: Technology, trends and challenges," *Renewable and Sustainable Energy Reviews*, vol. 114, p. 109336, 2019.

[4] K. Dang, J. Zhang, H. Zhou, S. Huang, T. Zhang, Z. Bian, Y. Zhang, X. Wang, S. Zhao, K. Wei, and Y. Hao, "A 5.8-GHz High-Power and High-Efficiency Rectifier Circuit With Lateral GaN Schottky Diode for Wireless Power Transfer," *IEEE Transactions on Power Electronics*, vol. 35, no. 3, pp. 2247–2252, Mar. 2020.

[5] T. Mishima and E. Morita, "High-Frequency Bridgeless Rectifier Based ZVS Multiresonant Converter for Inductive Power Transfer Featuring High-Voltage GaN-HFET," *IEEE Transactions on Industrial Electronics*, vol. 64, no. 11, pp. 9155–9164, Nov. 2017.

[6] S. Öztürk, P. Poşpoş, V. Utalay, A. Koç, M. Ermiş, and I. Çadırcı, "Operating principles and practical design aspects of all SiC DC/AC/DC converter for MPPT in grid-connected PV supplies," *Solar Energy*, vol. 176, no. October, pp. 380–394, Jul. 2018.

[7] M. Abbasi and J. Lam, "A Modular SiC-Based Step-Up Converter with Soft-Switching-Assisted Networks and Internally Coupled High-Voltage-Gain Modules for Wind Energy System with a Medium-Voltage DC-Grid," *IEEE Journal of Emerging and Selected Topics in Power Electronics*, vol. 7, no. 2, pp. 798–810, Jun. 2019.

[8] B. Li, Q. Li, F. C. Lee, Z. Liu, and Y. Yang, "A High-Efficiency High-Density Wide-Bandgap Device-Based Bidirectional On-Board Charger," *IEEE Journal of Emerging and Selected Topics in Power Electronics*, vol. 6, no. 3, pp. 1627–1636, Sep. 2018.

[9] H. Li, Z. Zhang, S. Wang, J. Tang, X. Ren, and Q. Chen, "A 300-kHz 6.6-kW SiC Bidirectional LLC Onboard Charger," *IEEE Transactions on Industrial Electronics*, vol. 67, no. 2, pp. 1435–1445, Feb. 2020.

[10] A. K. Morya, M. C. Gardner, B. Anvari, L. Liu, A. G. Yepes, J. Doval-Gandoy, and H. A. Toliyat, "Wide bandgap devices in AC electric drives: Opportunities and challenges," *IEEE Transactions on Transportation Electrification*, vol. 5, no. 1, pp. 3–20, Mar. 2019.

[11] A. Matallana, E. Ibarra, I. López, J. Andreu, J. I. Garate, X. Jordà, and J. Rebollo, "Power module electronics in HEV/EV applications: New trends in wide-bandgap semiconductor technologies and design aspects," *Renewable and Sustainable Energy Reviews*, vol. 113, p. 109264, Oct. 2019.

[12] G. Liu, K. Bai, M. McAmmond, A. Brown, P. M. Johnson, A. Taylor, and J. Lu, "Comparison of SiC MOSFETs and GaN HEMTs based high-efficiency high-power-density 7.2kW EV battery chargers," in *2017 IEEE 5th Workshop on Wide Bandgap Power Devices and Applications, WiPDA 2017*, Albuquerque, NM, USA, 2017, pp. 391–397.

[13] A. S. Abdelrahman, Z. Erdem, Y. Attia, and M. Z. Youssef, "Wide Bandgap Devices in Electric Vehicle Converters: A Performance Survey," *Canadian Journal of Electrical and Computer Engineering*, vol. 41, no. 1, pp. 45–54, Feb. 2018.

[14] A. Jafari, M. S. Nikoo, N. Perera, H. K. Yildirim, F. Karakaya, R. Soleimanzadeh, and E. Matioli, "Comparison of Wide-Band-Gap Technologies for Soft-Switching Losses at High Frequencies," *IEEE Transactions on Power Electronics*, vol. 35, no. 12, pp. 12 595–12 600, Dec. 2020.

[15] D. Han, S. Li, Y. Wu, W. Choi, and B. Sarlioglu, "Comparative Analysis on Conducted CM EMI Emission of Motor Drives: WBG Versus Si Devices," *IEEE Transactions on Industrial Electronics*, vol. 64, no. 10, pp. 8353–8363, Oct. 2017.

[16] J. Xu, J. Han, Y. Wang, M. Ali, and H. Tang, "High-Frequency SiC Three-Phase VSIs With Common-Mode Voltage Reduction and Improved Performance Using Novel Tri-State PWM Method," *IEEE Transactions on Power Electronics*, vol. 34, no. 2, pp. 1809–1822, Feb. 2019.

[17] Q. Yan and X. Yuan, "A Double-Modulation-Wave PWM for Dead-Time-Effect Elimination and Synchronous Rectification in SiC-Device-Based High-Switching-Frequency Converters," *IEEE Transactions on Power Electronics*, vol. 35, no. 12, pp. 13 500–13 513, Dec. 2020.

[18] D. Lumbreras, J. Zaragoza, N. Berbel, J. Mon, E. Galvez, and A. Collado, "Comprehensive Analysis of Hexagonal Sigma-Delta Modulations for Three-Phase High-Frequency VSC Based on Wide-Bandgap Semiconductors," *IEEE Transactions on Power Electronics*, in press.

[19] G. Luckjiff and I. Dobson, "Hexagonal $\Sigma\Delta$ modulators in power electronics," *IEEE Transactions on Power Electronics*, vol. 20, no. 5, pp. 1075–1083, Sep. 2005.

[20] D. Lumbreras, J. Zaragoza, J. Mon, E. Galvez, and A. Collado, "Efficiency analysis of wide band-gap semiconductors for two-level and three-level power converters," in *IECON 2019 - 45th Annual Conference of the IEEE Industrial Electronics Society*, Lisbon, Portugal, 2019, pp. 5126–5133.

[21] D. Holmes, "The significance of zero space vector placement for carrier-based PWM schemes," *IEEE Transactions on Industry Applications*, vol. 32, no. 5, pp. 1122–1129, Sep. 1996.

[22] S. Pavan, R. Schreier, and G. C. Temes, *Understanding Delta-Sigma Data Converters*, 2nd ed. Wiley-IEEE Press, 2017.

[23] J. C. Candy, "A Use of Double Integration in Sigma Delta Modulation," *IEEE Transactions on Communications*, vol. 33, no. 3, pp. 249–258, Mar. 1985.

[24] J. Reiss, "Understanding Sigma-Delta Modulation: The Solved and Unsolved Issues," *AES: Journal of the Audio Engineering Society*, vol. 56, no. 1/2, pp. 49–64, Jan. 2008.

[25] J. Pou, D. Osorno, J. Zaragoza, S. Ceballos, and C. Jaen, "Power losses calculation methodology to evaluate inverter efficiency in electrical vehicles," in *2011 7th International Conference-Workshop Compatibility and Power Electronics, CPE 2011 - Conference Proceedings*. Tallinn, Estonia: IEEE, 2011, pp. 404–409.